Chest Tells Who You Are: Feature Analysis of Wearable Near-Field Sensor Signals for Biometric Authentication

Shun Hinatsu
Mitsubishi Electric Corporation
Kamakura, Kanagawa, Japan
Hinatsu.Shun@bc.MitsubishiElectric.co.jp

Hidetoshi Makimura
Mitsubishi Electric Corporation
Kamakura, Kanagawa, Japan
Makimura.Hidetoshi@cw.MitsubishiElectric.co.jp

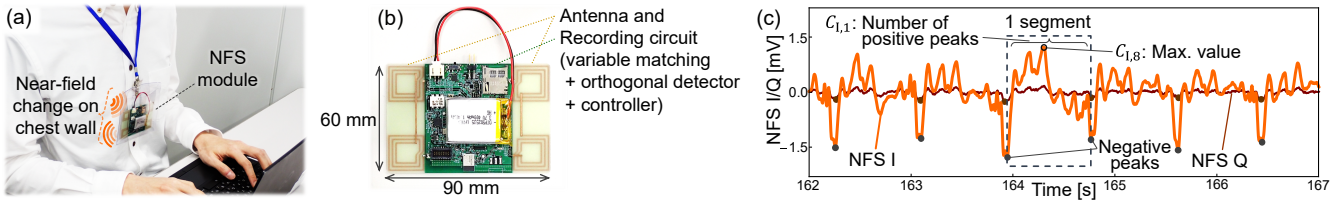

Figure 1: (a) Recording of near-field sensor (NFS) signals in an office. (b) NFS module used in the experiment. (c) Example of recorded NFS signals, along with extracted features, whose contributions to authentication were evaluated in this study.

ABSTRACT

We evaluated biometric authentication based on chest wall displacement recorded as time-series signals by a wearable near-field electromagnetic sensor (NFS) and on features extracted from those signals. NFSs can record near-field changes between the chest wall and the antenna with minimal restrictions; however, definitive fiducial features for these waveforms have not been established, yet are necessary for deployment in resource-constrained personalized systems. We collected NFS signals from 22 participants using an NFS module and defined 40 features to evaluate their contributions to authentication. We compared authentication performance across different feature combinations and models. A random forest model achieved the equal error rate of 0.065±0.066, while an extreme gradient boosting model achieved the fastest processing time.

CCS CONCEPTS

• **Human-centered computing** → **Ubiquitous and mobile computing systems and tools**.

KEYWORDS

Biometrics, Chest wall, Feature extraction, Near-field

ACM Reference Format:
Shun Hinatsu and Hidetoshi Makimura. 2026. Chest Tells Who You Are: Feature Analysis of Wearable Near-Field Sensor Signals for Biometric Authentication. In *Proceedings of Everyday Wearable for Personalized Health and Well-Being Workshop at CHI 2026 (CHI '26 Workshop).* ACM, New York, NY, USA, 4 pages. https://doi.org/XXXXXXX.XXXXXXX

CHI '26 Workshop, April 14, 2026, Barcelona, Spain

ACM ISBN 978-1-4503-XXXX-X/2018/06…$15.00
https://doi.org/XXXXXXX.XXXXXXX

1 INTRODUCTION

Near-field electromagnetic sensors (NFSs) can detect several physiological phenomena in humans. An NFS uses a small antenna to sense minute near-field changes, which are manifested as variations in antenna impedance, without requiring skin contact. It detects motions of underlying organs (e.g., cardiac activity) rather than surface skin displacement [4, 10], offering advantages over other heartbeat measurement techniques such as electrocardiography (ECG) and photoplethysmography (PPG) in terms of non-contact operation and robustness to ambient light. Our previous works developed an NFS module for heartrate monitoring [14] (Fig. 1(a)), and an authentication system using that module [3] based on studies showing that waveforms recorded by these techniques exhibit individual characteristics [4, 10, 14]. Time-series physiological signals such as ECG and NFS signals may enable seamless integration of biomedical monitoring and authentication in personalized systems [12, 13].

Signal-processing techniques for user authentication using time-series physiological signals are broadly categorized as fiducial or non-fiducial [12]. Fiducial methods focus on waveform morphology (e.g., positive and negative peaks) and extract those landmarks from signal segments as features, which are also important for physiological interpretation [7]. Non-fiducial methods apply mathematical computations or machine learning such as frequency analysis or deep learning techniques to segments [5, 8, 12], whose outputs can be harder to interpret. To the best of our knowledge, no study (including our previous work [3]) has explicitly defined and evaluated fiducial features for NFS waveforms; this gap is partly because NFSs have been less widely available and prior work has emphasized frequency-domain analysis for biomedical applications [4, 10]. Further investigation of NFS signal processing for both authentication and biomedical applications is needed, with attention to lightweight algorithmic optimization and physiological interpretability in resource-constrained personalized systems [13].

In this work, we investigate fiducial features in NFS signals and evaluate their contributions to authentication to derive an optimized algorithm. Our contributions are summarized as follows:

Table 1: Features extracted from NFS signals with importance ranks in authentication in each recording state.

Ref.	ID	Abstract	Meanings	Importance rank (rest, speak, type) RF (I/Q)	XGB (I/Q)
[2]	$C_{I/Q,1}$	Number of positive peaks	Complexity of displacement	36, 33, 34 / 11, 24, 25	19, 13, 17 / 6, 9, 16
	$C_{I/Q,2}$	Positive slant of first peak	Displacement velocity	32, 14, 18 / 9, 20, 21	24, 27, 27 / 22, 21, 24
	$C_{I/Q,3}$	Negative slant of final peak	Displacement velocity	33, 18, 20 / 12, 21, 17	26, 25, 28 / 33, 23, 22
	$C_{I/Q,4}$	Time interval	Displacement velocity	38, 32, 31 / 25, 22, 23	28, 33, 33 / 15, 17, 19
[7]	$C_{I/Q,5}$	Mean value	Average of displacement in one period	39, 28, 29 / 16, 27, 28	34, 31, 30 / 1, 11, 11
	$C_{I/Q,6}$	Standard deviation	Change in displacement in one period	21, 9, 12 / **4**, 13, 8	9, 12, 12 / 12, 8, 6
	$C_{I/Q,7}$	Mean of DTW distance	Change in displacement in one session	10, **1**, **3** / **5**, **5**, **4**	**5**, **1**, **4** / **3**, **5**, **3**
	$C_{I/Q,8}$	Max. value	Peak of displacement	27, 10, 15 / 7, 16, 13	27, 26, 26 / 29, 10, 18
	$C_{I/Q,9}$	Min. value	Peak of displacement	14, 7, 6 / **2**, 19, 10	**4**, 18, 10 / 17, 15, 8
	$C_{I/Q,10}$	Time which has $C_{I/Q,8}$	Displacement velocity	37, 31, 32 / 22, 23, 24	23, 34, 34 / 11, 28, 15
	$C_{I/Q,11}$	Time which has $C_{I/Q,9}$	Displacement velocity	40, 37, 37 / 29, 35, 36	35, 35, 35 / 25, 32, 36
	$C_{I/Q,12}$	Max. of wavelet coefficients	Frequency characteristics of displacement	26, 11, 16 / 8, 15, 14	20, 22, 37 / 31, 7, 20
	$C_{I/Q,13}$	Min. of wavelet coefficients	Frequency characteristics of displacement	15, 8, 7 / 6, 17, 11	10, 16, 14 / 18, 20, 7
	$C_{I/Q,14}$	Skewness	Displacement velocity	34, 29, 30 / **3**, 26, 27	14, 30, 31 / 16, 24, 29
	$C_{I/Q,15}$	Kurtosis	Displacement velocity	35, 30, 33 / **1**, 25, 26	32, 29, 32 / **2**, 19, 21
[6]	$C_{I/Q,16}$	PSD of 0.5 - 4.0 Hz	Frequency characteristics of displacement	30, 12, 19 / 20, 34, 22	30, 14, 23 / 36, 36, 13
	$C_{I/Q,17}$	PSD of 4.0 - 8.0 Hz		24, 6, 9 / 19, 38, 35	13, 6, 9 / 37, 37, 25
	$C_{I/Q,18}$	PSD of 8.0 - 14.0 Hz		28, **4**, **5** / 18, 39, 38	8, **4**, **5** / 37, 38, 38
	$C_{I/Q,19}$	PSD of 14.0 - 30.0 Hz		31, **3**, **1** / 18, 39, 38	21, **3**, **2** / 37, 38, 39
	$C_{I/Q,20}$	PSD of 30.0 Hz -		23, **2**, **2** / 13, 37, 40	7, **2**, **1** / 37, 38, 40

- We define a total of 40 fiducial features in NFS signals relevant to user authentication.
- We recorded these features from 22 participants' NFS signals under three recording states and compared them.
- We evaluate the contribution of these features to authentication to achieve great authentication performance.

2 EXPERIMENT

Figure 2 presents an overview of the experimental procedure. We recorded NFS signals, trained and tested authentication models while varying the combinations of features extracted from them.

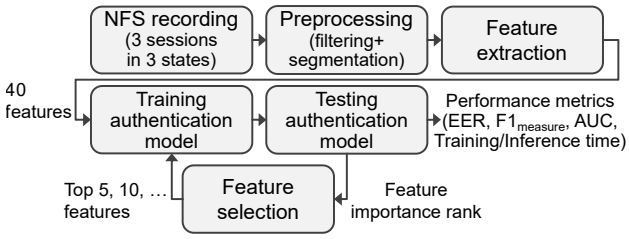

Figure 2: Experimental procedure.

2.1 Experimental Setup and NFS Recording

NFS signals were recorded from 22 participants (IDs: P1, P2, ..., P22; 10 females and 12 males; aged between their 30s and 50s) who did not have any cardiac diseases. The NFS module was placed on the chest over clothing, and single-lead ECG electrodes were attached to the skin as a reference. The module incorporates a four-element loop antenna operating in the very-high-frequency (VHF) band (30-300 MHz) and a battery-powered circuit. VHF radio waves undergo low attenuation in biological tissue, and the antenna's low radiation efficiency makes the system relatively insensitive to external interference. The antenna senses chest wall displacement as changes in input impedance, which can transmit and receive continuous waves centered at 100 MHz. A variable matching circuit adaptively adjusts capacitance based on the orthogonal In-phase/Quadrature-phase (I/Q) outputs from the detector, maintaining stable recordings [14]. The signals were recorded in three states: resting, speaking, and typing on a PC keyboard, to evaluate authentication feasibility in conditions typical for office work. Recordings were obtained at a 250 Hz sampling rate in three 180-s sessions per state, with a few minutes intervals. Data were processed with an Intel Core i5-10210U CPU, 64 GB RAM, and an NVIDIA GeForce RTX 3070 GPU (32 GB VRAM), using PyTorch 2.6.0 and CUDA 11.8. All procedures were approved by the Ethical Committee of the Information Technology R&D Center (2023-B001) of Mitsubishi Electric Corporation, Japan, and informed consent was obtained from all participants.

2.2 Preprocessing and Feature Extraction

After applying a fourth-order Butterworth filter with a frequency bandwidth of 1-40 Hz and segmentation using two negative peaks to the recorded signals in the preprocessing, we extracted 40 features $C_{I/Q,1}, C_{I/Q,2}, ..., C_{I/Q,20}$ from the I/Q segments, as shown in Fig. 1(c). Table 1 lists the features, which are signal-type independent and were selected based on studies using physiological signals for authentication [2, 6, 7] as follows:

- $C_{I/Q,1}$, ..., $C_{I/Q,4}$ [2] are the peak-related features.
- $C_{I/Q,5}$, ..., $C_{I/Q,15}$ [7] are mainly statistical metrics and include the mean dynamic time warping (DTW) distance, which quantifies similarity between time-series segments.
- $C_{I/Q,16}$, ..., $C_{I/Q,20}$ [6] are power spectral density (PSD) features computed by the Fourier transform. The frequency bandwidths are based on electroencephalogram signals [1].

2.3 Authentication Model and Feature Selection

To evaluate authentication performance using the extracted features, we employed two decision tree-based classifiers as authentication models: random forest (RF) and extreme gradient boosting (XGB), which have been successfully applied to authentication using physiological signals [6, 13]. Additionally, the libraries we used provide feature-ranking functions that indicate each feature's importance [9, 15]; we used these rankings to modify feature combinations such as top 5, 10, ... features for training and testing. In comparison, we also developed two deep learning models using one segment as non-fiducial features: a one-dimensional convolutional neural network (CNN) model including three convolutional layers [8], and a combination of CNN and long short-term memory (LSTM) including two convolutional layers and two LSTM blocks (CNN+LSTM) [5]. We conducted three-fold cross-validation in which two folds were used for training and one fold for testing from three sessions in each recording state. We computed the equal error rate (EER), $F1_{measure}$ and the area under the receiver operating characteristic (ROC) curve (AUC) as performance metrics. We also recorded the training and inference time for each model.

3 RESULTS AND DISCUSSION

3.1 Authentication Performance

Figure 3 (left) shows examples of NFS I/Q and ECG signals recorded in the experiment; the signals exhibit similar cyclical increases and decreases. Figure 3 (right) shows examples of the PSDs of the NFS signals, demonstrating that spectral peaks in the NFS align with those in the ECG. Features in Figs. 3(a) and (b) suggest person-specific differences, such as skewness and PSD distributions, indicating the potential for the features in NFS signals for authentication.

Table 2 compares authentication performance across models and states. RF using all 40 fiducial features achieved the best EER and AUC compared with the other models, including deep learning models that use non-fiducial features. The models tended to perform worse in non-resting states than in the resting state. Table 3 reports training and inference times for each model in the resting state. XGB with the 40 fiducial features achieved the best (fastest) training and inference times among the authentication models.

3.2 Evaluation of Features

Table 1 also lists the importance rank of each feature in each recording state. Smaller rank values indicate greater importance; ranks 1–5 are shown in bold. Figure 4 shows correlation coefficients for all pairs of features extracted from the I and Q signals, indicating correlations among some feature pairs, especially ones in the same references, and suggesting that removing redundant features may be advisable. For example, the DTWs from the I/Q signals ($C_{I/Q,7}$), which receive high ranks in Table 1, correlate with several features

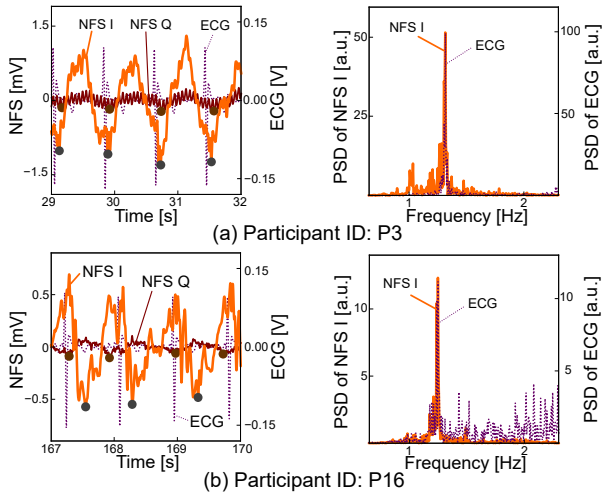

Figure 3: Examples of recorded signals. Left: NFS I/Q and ECG signals. Right: PSD of NFS I and ECG signals.

Table 2: Comparison of authentication performance metrics across models and states. The best values are in bold.

Model	State	EER	$F1_{measure}$	AUC
CNN	Rest	0.067±0.053	**0.887±0.082**	0.962±0.046
	Speak	0.116±0.069	0.800±0.122	0.939±0.057
	Type	0.086±0.053	0.849±0.100	0.961±0.034
CNN+ LSTM	Rest	0.066±0.049	0.884±0.081	0.967±0.039
	Speak	0.108±0.066	0.849±0.100	0.961±0.034
	Type	0.085±0.054	0.876±0.082	0.962±0.034
RF w/ 40 features	Rest	**0.065±0.066**	0.857±0.120	**0.967±0.047**
	Speak	0.108±0.058	0.745±0.120	0.943±0.042
	Type	0.074±0.048	0.810±0.105	0.966±0.032
XGB w/ 40 features	Rest	0.070±0.069	0.847±0.130	0.957±0.058
	Speak	0.094±0.043	0.781±0.107	0.954±0.032
	Type	0.069±0.053	0.855±0.089	0.965±0.050

Table 3: Training and inference time by each model.

Model	Training time [s]	Inference time [s]
CNN	29.110±2.383	1.528±3.262
CNN +LSTM	36.257±2.027	0.040±0.011
RF w/ 40 features	6.878±3.037	0.484±0.040
XGB w/ 40 features	**0.218±0.138**	**0.006±0.002**

in [7]. Comparing resting and non-resting states (speaking and typing), the high-frequency PSDs from the I signals ($C_{I,18}$-$C_{I,20}$) contributed to performance in non-resting states. In contrast, skewness and kurtosis from the Q signals ($C_{Q,14}$ and $C_{Q,15}$) contributed little in non-resting states, possibly because those high-frequency components distorted the waveforms. Figure 5 shows the relationship between AUC, EER and the number of features for the models.

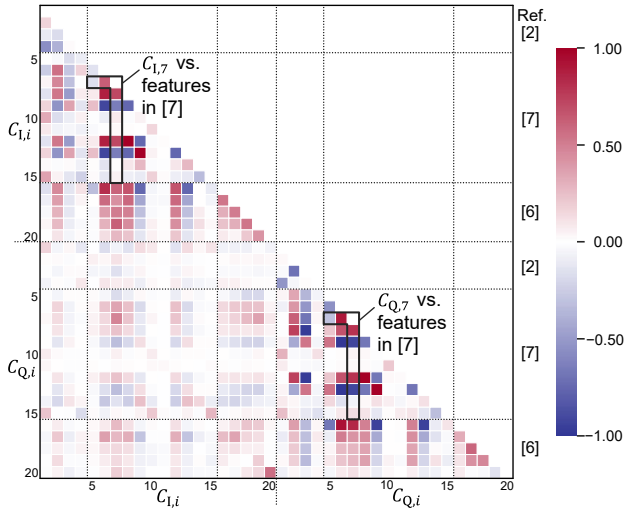

Figure 4: Correlation coefficients between all pairs of features ($C_{I,1}$, ..., $C_{I,20}$, $C_{Q,1}$, ..., $C_{Q,20}$) extracted from NFS I/Q signals.

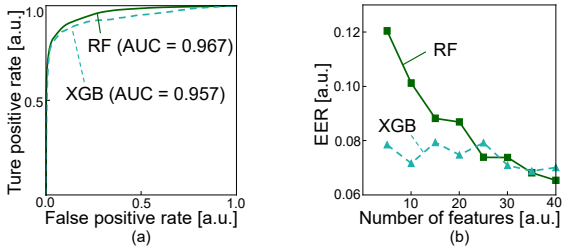

Figure 5: (a) ROC curve using RF and XGB with 40 features. (b) Relationship between the EER and the number of features.

As more features were added according to their ranking, both models' performance tended to improve; however, XGB performed well even with a small number of features. Considering the processing times reported in Table 3, XGB may be the more efficient option.

3.3 Experimental Limitation and Future Works

Although our current system recorded NFS signals and performed segmentation and preprocessing on a PC for input to the models used in the experiment, implementing model-related processing on the NFS module itself could improve usability. On such a module, all processing should be optimized; for example, peak detection should use real-time algorithms [11]. Miniaturizing the module (antenna and circuitry) would enable recordings from multiple body sites and facilitate everyday use, similar to a wearable ECG accessory [16]. Our experiment used healthy participants and the present setup; future work will collect data from participants with cardiac conditions using an optimized system, where obtaining clean single-cycle segments and extracting fiducial features may be more challenging in personalized systems. Addressing these challenges will require more robust segmentation, feature extraction and validation under diverse, real-world conditions to evaluate the feasibility of the authentication using the fiducial features.

4 CONCLUSION

We evaluated biometric authentication using chest-wall displacement time-series recorded by a wearable NFS and fiducial features extracted from those signals. NFS I/Q signals were collected from 22 experimental participants, and 40 fiducial features were analyzed to assess their contributions and to identify effective feature sets and authentication models. RF achieved the lowest EER of 0.065±0.066, while XGB provided the fastest processing times and robust performance with a small feature set compared with the other models. Future work will focus on on-device model processing, further hardware miniaturization, and validating the approach with participants who have cardiac conditions to assess feasibility under more challenging, real-world conditions.

REFERENCES

[1] Patricia Arias-Cabarcos, Thilo Habrich, Karen Becker, Christian Becker, and Thorsten Strufe. 2021. Inexpensive brainwave authentication: new techniques and insights on user acceptance. In *Proceedings of the 30th USENIX Security Symposium (USENIX Security)*. 55–72.

[2] Yicheng Gu, Yuanting Zhang, and Yuan-Ting Zhang. 2003. A novel biometric approach in human verification by photoplethysmographic signals. In *Proceedings of the 4th International IEEE EMBS Special Topic Conference on Information Technology Applications in Biomedicine (ITAB)*. 13–14.

[3] Shun Hinatsu and Hidetoshi Makimura. 2025. Comparative evaluation of non-fiducial techniques toward user authentication by noncontact electromagnetic sensor on chest wall. *IEEE Sensors Letters* 9, 11 (2025), 7005504.

[4] Dong-Yu Hsu, Yen-Ling Sung, Shih-Hua Ni, Chiu-Yun Huang, Yu-Xiang Huang, En-Zhu Lyu, Chun-Hsien Chen, and Ting-Wei Wang. 2024. Wearable pocket-sized fully non-contact biomedical eddy current sensor for simultaneous cardiac and lung monitoring. *IEEE Transactions on Instrumentation and Measurement* 73 (2024), 4007213.

[5] Dae Yon Hwang, Bilal Taha, and Dimitrios Hatzinakos. 2021. PBGAN: Learning PPG representations from GAN for time-stable and unique verification system. *IEEE Transactions on Information Forensics and Security* 16 (2021), 5124–5137.

[6] Ryo Iijima, Tatsuya Takehisa, Tetsushi Ohki, and Tatsuya Mori. 2024. The catcher in the eye: Recognizing users by their blinks. In *Proceedings of the 19th ACM Asia Conference on Computer and Communications Security (ASIACCS)*. 1739–1752.

[7] Vasu Jindal, Javad Birjandtalab, M Baran Pouyan, and Mehrdad Nourani. 2016. An adaptive deep learning approach for PPG-based identification. In *Proceedings of the 2016 38th Annual International Conference of the IEEE Engineering in Medicine and Biology Society (EMBC)*. 6401–6404.

[8] Yejin Kim, Gyuho Choi, and Chang Choi. 2023. One-dimensional shallow neural network using non-fiducial based segmented electrocardiogram for user identification system. *IEEE Access* 11 (2023), 102483–102491.

[9] Scikit Learn. 2025. RandomForestClassifier-scikit-learn 1.8.0 documentation. https://scikit-learn.org/stable/modules/generated/sklearn.ensemble.RandomForestClassifier.html Retrieved February 17, 2026.

[10] Noor Mohammed, Kim Cluff, Mark Sutton, Bernardo Villafana-Ibarra, Benjamin E Loflin, Jacob L Griffith, Ryan Becker, Subash Bhandari, Fayez Alruwaili, and Jaydip Desai. 2022. A flexible near-field biosensor for multisite arterial blood flow detection. *Sensors* 22, 21 (2022), 8389.

[11] Jiapu Pan and Willis J Tompkins. 2007. A real-time QRS detection algorithm. *IEEE Transactions on Biomedical Engineering* BME-32, 3 (2007), 230–236.

[12] João Ribeiro Pinto, Jaime S Cardoso, and André Lourenço. 2018. Evolution, current challenges, and future possibilities in ECG biometrics. *IEEE Access* 6 (2018), 34746–34776.

[13] Danyal Shahmirzadi and Wen Fong Wang. 2026. Concise PPG features for lightweight identity verification. *Multimedia Tools and Applications* 85, 2 (2026), 147.

[14] Saki Wada, Kengo Nishimoto, Yoshio Inasawa, and Shintaro Izumi. 2023. Estimated results of RR interval using a small card-sized VHF-band contactless heartbeat sensor module. In *Proceedings of the IEEE 19th International Conference on Body Sensor Networks (BSN)*. 1–4.

[15] xgboost developers. 2026. XGBoost Documentation — xgboost 3.2.0 documentation. https://xgboost.readthedocs.io/en/release_3.2.0/ Retrieved February 17, 2026.

[16] Qiuyue Xue, Eric Steven Martin, Jiaqing Liu, Ruiqing Wang, Antonio Glenn, Richard Li, Vikram Iyer, and Shwetak Patel. 2025. ECG Necklace: Low-power Wireless Necklace for Continuous ECG monitoring. In *Proceedings of the 2025 CHI Conference on Human Factors in Computing Systems (CHI)*. 1–14.

Received 27 February 2026; revised ; accepted